Applied Energy 101 (2013) 151–160

Contents lists available at SciVerse ScienceDirect

Applied Energy

journal homepage: www.elsevier.com/locate/apenergy

Harvesting high altitude wind energy for power production: The concept based on Magnus' effect

Luka Perković [a,*], Pedro Silva [b], Marko Ban [a], Nenad Kranjčević [c], Neven Duić [a]

[a] Department of Energy, Power Engineering and Environment, Faculty of Mechanical Engineering and Naval Architecture, Ivana Lučića 5, 10000 Zagreb, Croatia
[b] Omnidea Lda, Rua Nova da Balsa, Lote D, Loja 5, 3510-007 Viseu, Portugal
[c] Department of Design, Faculty of Mechanical Engineering and Naval Architecture, Ivana Lučića 5, Zagreb, Croatia

HIGHLIGHTS

- ▶ High altitude wind energy as a great potential for energy source in the near future.
- ▶ Magnus' effect can be used for harvesting high altitude winds for energy production.
- ▶ We showed a theoretical feasibility study of Magnus' effect as a concept for harvesting high altitude winds.

ARTICLE INFO

Article history:
Received 9 December 2011
Received in revised form 10 June 2012
Accepted 21 June 2012
Available online 20 July 2012

Keywords:
Magnus' effect
Renewable energy sources
High altitude wind energy
Computational fluid dynamics

ABSTRACT

High altitude winds are considered to be, together with solar energy, the most promising renewable energy source in the future. The concepts based on kites or airfoils are already under development. In this paper the concept of transforming kinetic energy of high altitude winds to mechanical energy by exploiting Magnus effect on airborne rotating cylinders is presented, together with corresponding two-dimensional per-module aerodynamic and process dynamics analysis. The concept is based on a rotating airborne cylinder connected to the ground station with a tether cable which is used for mechanical energy transfer. Performed studies have shown the positive correlation between the wind speed and mechanical energy output. The main conclusion of this work is that the presented concept is feasible for power production.

1. Introduction

1.1. Motivation and the potential of high altitude winds for power production

The constant need for reduction of emissions and dependency on oil has made research, development, production and installation of renewable energy sources economically viable during the past decades [1–3]. In addition to solar and hydro, one of the most relevant renewable energy sources is wind. All feasible concepts for exploiting wind for power production are currently restricted to terrestrial winds. World's largest wind turbine reaches top height of little less than 200 m (Enercon E-126 with rated capacity of 7.58 MW). Wind power density in these areas is generally under the influence of relief (mountains, hills, valleys), ground thermic (thermal capacity of different soils and water) and coverage type (vegetation) [4]. It is clear that in higher regions wind is less influential by those parameters. They become steadier, more persistent and of higher velocity magnitude [5]. This means that development of concepts which aim to harvest winds on these heights may result in new and powerful category of renewable energy sources. These concepts are called high altitude wind energy (HAWE) or high altitude wind power (HAWP) systems. Wind power density which stands on disposal for power production is a function of air density and wind velocity. Profile of wind power density with respect to height, covering average for the entire world as well as some large cities, was assessed for the first time by Archer and Caldeira in 2009 [6] for altitudes between 500 and 12,000 m. However, distribution over the Earth's surface shows significant difference over the longitude and latitude, see Fig. 1.

Wind power density in work of Archer and Caldeira [6] is based on reanalysis data from the National Centers for Environmental Prediction (NCEP) and the Department of Energy (DOE) [7]. In this work the same data for the approximation of wind profile is used. The same dataset can be used for estimating wind power on terrestrial level (example of 10 m above ground level in Hagspiel et al. [8]).

* Corresponding author. Fax: +385 1 6156 940.
E-mail addresses: Luka.Perkovic@fsb.hr (L. Perković), Pedro.Silva@omnidea.net (P. Silva), Marko.Ban@fsb.hr (M. Ban), Nenad.Kranjcevic@fsb.hr (N. Kranjčević), Neven.Duic@fsb.hr (N. Duić).

0306-2619/$ - see front matter © 2012 Elsevier Ltd. All rights reserved.
http://dx.doi.org/10.1016/j.apenergy.2012.06.061

Nomenclature

Latin

A	cylinder cast surf. (m^2)
C	model coeffi.
CF_L	lift force coeff.(–)
CF_D	drag force coeff.(–)
CM_Z	moment coeff(–)
D	cylinder diameter (m)
E	model constant (–)
E_{net}	net energy (J)
F_c	cable force (N)
F_g	net weight on ABM (N)
$F_{g,c}$	cable weight (N)
$F_{g,ABM}$	ABM weight (N)
$F_{g,EM}$	EM weight (N)
F_l	net lift on ABM (N)
$F_{L,Ar}$	buoyant lift force (N)
F_w	wind force (N)
$F_{w,D}$	wind force, drag (N)
$F_{w,L}$	wind force, lift (N)
g	gravitation const. (m/s^2)
K	model constant (N s/m)
k_p	first-node turbulence (m^2/s^2)
L	cylinder length (m)
L_c	cable length (m)
M_{fr}	friction moment (N m)
M_{el}	moment of el. motor (N m)
n	freq. of cylinder rot. (1/s)
n_{max}	maximum allowable n (1/s)
$\vec{n}$	normal vector (–)
p	pressure (N/m^2)
P_c	cable power (W)
P_{EM}	EM power (W)
P_{net}	net power (W)
$q_{g,c}$	spec. cable weight (N/m)
$q_{g,cast}$	spec. cast weight (N/m^2)
R	cylinder radius (m)
t	time (s)
U_p	first-node velocity (m/s)
U_w	cylinder wall velocity (m/s)
V	cylinder volume (m^3)
v	ABM velocity (m/s)
$\vec{v}'_c$	thresh. velocity (m/s)
v_{rel}	relative velocity (m/s)
v_w	wind velocity (m/s)
v_{II}	ABM velocity comp. (m/s)
$\vec{x}$	ABM horiz. pos. (m)
X	spin ratio (–)
X_{opt}	optimum spin ratio (–)
$\vec{y}$	ABM vert. pos. (m)
y^*	friction length (–)
y_p	first-node distance (m)

Greek

α	angle (rad)
α'	critical angle (rad)
μ	dynamic viscosity (Pa s)
ρ	density (kg/m^3)
τ	process time (s)
$\tau_{wall,shear}$	wall shear stress (N/m^2)
ω	cylinder rotation (1/s)
ω_{max}	maximum allowable ω (1/s)

1.2. Short overview of HAWE concepts

Bronstein in 2011 made a positive correlation between advancement in development of high altitude wind energy (HAWE) systems to the price of oil [4]. Same author stated that present state of development in concepts for capturing high altitude wind power still encounters many technical and policy difficulties. The best proof for this is that, by authors' knowledge, only the Magenn's air rotor system [9] is available for ordering on the market. Up to date, all concepts for harvesting high altitude winds for power production are currently in research and development stage, with some in the prototype phase. Lansdorp and Ockels in 2005 compared laddermill and pumping mill concepts by weight criteria [10]. Roberts et al. in 2007 presented a 240 kW concept of tethered rotorcraft [11]. High altitude kites are one of the prevailing concepts in the literature. Loyd in 1980 performed calculations for power production by using the kite concept and validated the results against simple analytical models [12]. Argatov et al. in 2009 made an estimation of the mechanical energy output [13] and Argatov and Silvennoinen in 2010 introduced the performance coefficient [14] for the same concept. Thesis of Fagiano in 2009 [15] showed that tethered airfoil concept (KiteGen) can be successfully used in power production on almost all locations in the world with costs lower than fossil energy. Kite concept is also explored by Canale et al. in 2009 [16]. Argatov et al. in 2011 presented analytical model of wind load on a tether constraining a power kite performing a fast crosswind motion [17]. Dirigible based rotor (DBR) are also under research, with Magenn air rotor system (M.A.R.S.) as most advanced example [9].

1.3. HAWE systems and energy planning

From the energy planning point of view, all HAWE systems are producing power in discontinuous cycles, having the production and recovery phase. This gives additional importance to energy storage systems, besides the ones arising from possible intermittency of the wind source or limitations of the grid. Krajačić et al. in 2011 related development and use of energy storage systems with feed-in tariffs [18]. Therefore, in the case of HAWE systems feed-in tariffs can play significant role, despite higher energy potential from high winds. Since up to date there are no analyses dealing with potential of power production from HAWE systems, it is unknown what would be the impact of incorporating these systems into energy systems throughout the world. However, motivation for that could be the increase in fossil fuel price, as well as CO_2 price. Since operating costs of the conventional systems rise with the increase in CO_2 price [19], the larger penetration of RES is allowed, possibly also with HAWE systems. HAWE systems could be used during the planning of electricity and/or integrated electricity and water supply. For example, they could be incorporated into the Renewislands methodology (Chen et al. in 2007 [20], Duić et al. in 2008 [21]), and the widely-used H2RES and EnergyPLAN models [22–26], by possibly using the same analogy with terrestrial winds. The difficulties are, though, in finding the real power potential from high winds and unknown response of HAWE systems to available wind potential, since the latter it still known only from modelling and simulation. In this work modelling of such response is done for HAWE concept based on Magnus' effect.

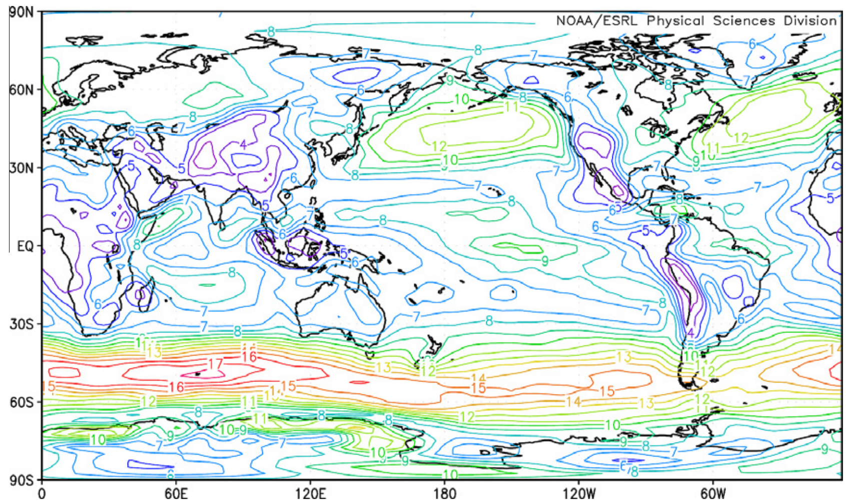

Fig. 1. Wind magnitude on pressure level of 850 mbar (corresponds to approx. 1500 m).

1.4. The overview of the concept based on Magnus' effect

The concept presented in this work has been designed in Omnidea Lda (Portugal) and is currently under initial, 'proof-of-concept' development stage within the scope of Seventh Framework Programme project called High Altitude Wind Energy (HAWE) [27]. The process of power production is based on reverting the drag force of the wind into lift force, which then results in lifting the so-called airborne module (ABM), see Fig. 2. This is done by rotating the cylinder in order to produce Magnus' effect which would revert some of the drag force into the lift. This process is done in the following way: rotating cylinder will tend to rotate surrounding viscous air, i.e. it will create boundary layer around itself. If apparent wind is streaming on the cylinder, its velocity field is superimposed to the induced velocity field by the cylinder's rotation. On the side of the cylinder where two velocity fields are opposing each other higher pressure area will occur, due to stagnation of the added velocity fields. On the other side of the cylinder lower pressure region will occur because two velocity fields are there supporting each other. Magnus' effect phenomenon was described in mid 19th century [28]. It is mainly a function of Re number based on cylinder diameter and spin ratio X, defined as $X = v_t/v_{rel}$. Based on velocities occurring in atmosphere up to 2000 m in height and cylinder diameter in the case presented in this paper, Re number values are between Re = 5.e05 and Re = 5.e06. These values fall under the high Re number regime. In 2001 Aoki and Ito performed some measurements of the flow past a circular cylinder [29]. In addition to that, numerical calculations in both Reynolds-averaged Navier Stokes (RANS) [30], and large eddy simulation (LES) framework [31–34] for high Re number have been performed. Generally, there is a lack of published data dealing with flow past rotating cylinder in the regime of high Re numbers [30].

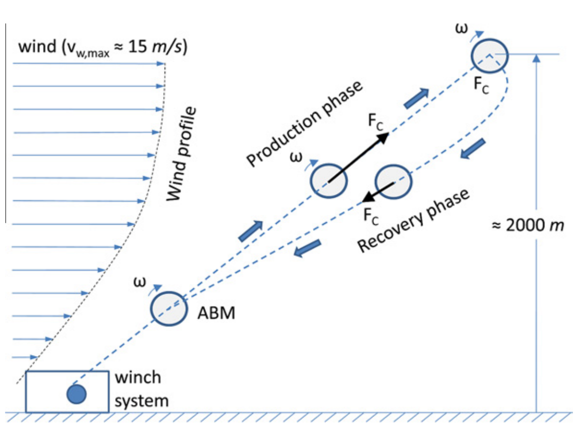

Fig. 2. Schematic view of the concept based on Magnus' effect.

ABM is connected with a cable to the winch system placed on a ground. Production is not continuous, but cyclic per unit. Each cycle consists of two phases: production and recovery phase. Cylinder of the ABM is filled with helium, making the whole airborne structure lighter than the air. This enables the ABM to have some starting height at the beginning of the process. Production phase occurs when ABM tends to move away from the winch system thus unwinding the cable. If winch is connected to generator, it will produce electricity. During the recovery phase generator enters into electro motor regime and pulls the cable back towards the drum and returning the ABM to starting position. The process of power production is successful if there is a surplus of energy left after recovery phase. Study performed in this paper shows that this surplus can be achieved and that it positively correlates with magnitude of the relative wind speed.

2. Simulation methodology

Modelling of the proposed concept was done on a several levels of computational simulations. Computational fluid dynamics (CFD) finite volume approach was used in order to get lift, drag and moment coefficients as a function of cylinder rotation and apparent wind speed. Both spatial and temporal discretization errors were reduced to minimum by performing calculations on several meshes with different cell sizes and time steps, where solution independent on these parameters was found. Modelling and numerical errors were not estimated nor specially treated. There are some indications that for simulation of the flow over the cylinder in supercritical regime, when Reynolds number is above 10^6, spanwise dimension can be neglected, making 3rd dimension unnecessary to model. According to Karabelas et al. [30], in supercritical region drag coefficient increases with Re number due to the action of the turbulence shear stresses. At the same time, according to some other studies, the shear-layer instability is predominantly two-dimensional (Singh and Mittal in 2005 [35], Mittal in 2001 [36], Braza et al. in 1990 [37]). Since operating Re number in this work is mainly in supercritical region, flow symmetry in spanwise direction is assumed. Therefore, CFD results were obtained from the solution of two-dimensional Navier–Stokes equations. This assumption was taken into account by some other publications dealing with numerical simulations of flow over the cylinder [30,35–37]. Coefficients resulting from CFD approach were then used as input parameters in the form of look-up tables for the simulation of the process, i.e. for the simulation of one cycle of the production and recovery phase. Process dynamics was done in the framework of integral parameters, where integration was only performed in time. CFD code used was AVL FIRE and solving of the ODE equations was performed in Matlab.

2.1. Lift, drag and moment of the airborne module (ABM)

Two-dimensional CFD calculations or rotating cylinder were performed in order to provide tables relating lift, drag and shear moment coefficients (CF_L, CF_D, CM_Z) as a function of Re number based on ABM cylinder diameter and ABM spin ratio (X):

$$CF_L, CF_D, CM_Z = f(X) \tag{1}$$

$$\mathrm{Re} = D\rho v_w/\mu \tag{2}$$

$$X = \omega R/v_{rel}, \tag{3}$$

where relative velocity is given by subtraction of ABM velocity from the wind velocity. If ABM is not moving, then $v_{rel} = v_w$.

$$\vec{v}_{rel} = \vec{v}_w - \vec{v} \tag{4}$$

Coefficients have the following definition:

$$CF_L = F_{w,L}/(0.5\rho v_{rel}^2 DL) \tag{5}$$

$$CF_D = F_{w,D}/(0.5\rho v_{rel}^2 DL) \tag{6}$$

$$CM_Z = M/(0.5\rho v_{rel}^2 \pi (D/2)^2 L) \tag{7}$$

Wind force is provided from the CFD calculation as a surface integral of pressure field over the complete cylinder surface:

$$\vec{F}_w = \int_A p(A) d\vec{A} = \vec{F}_{w,L} + \vec{F}_{w,D} \tag{8}$$

Wall shear stress is determined in the common way:

$$\tau_{wall,shear} = \mu(U_p - U_w)\big|_{||}/y_p \tag{9}$$

2.1.1. CFD calculation set-up

Turbulence framework of the CFD calculations is LES adopted for two-dimensional set-up. Solver for incompressible flow is used. In LES it is possible to directly simulate turbulent vortices larger than the filter size. Filter size is determined by node spacing of the grid. Part of the turbulence that has to be modelled is turbulence related to the characteristic length scale which is smaller than the filter size, the so-called sub-grid scale (SGS) turbulence. SGS model used in this work is based on coherent structures and it was introduced by Kobayashi in 2005 [38]. The approach relates SGS turbulence to the eddy-viscosity which is modelled by a coherent structure function (CSF) with a fixed model parameter. Eddy viscosity is added to the molecular viscosity in Navier–Stokes equations. Detailed description of the model, as well as validation cases can be found in reference paper [38].

For wall treatment no-slip wall conditions were used. Cylinder is assumed to be smooth. Rotation of the cylinder was done by adding velocity components to the cylinder walls by using formula $\vec{v} = \vec{\omega} \times \vec{R}$.

Velocity is prescribed on inlet boundary condition and static pressure is prescribed on the outlet boundary. Boundary conditions are set to the distance of 80D from the cylinder surface.

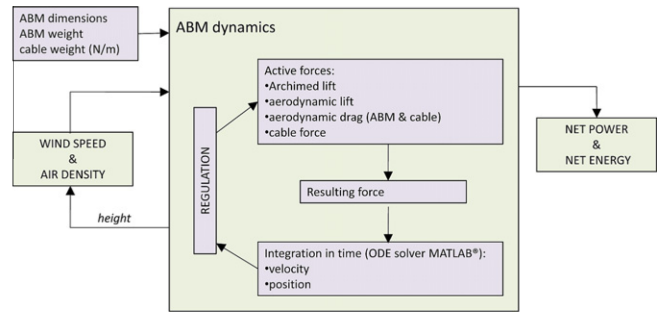

Fig. 3. Process dynamics modelling scheme.

2.2. Process dynamics

Schematic view of process dynamics modelling is given in Fig. 3. ABM dimensions and weight, as well as cable weight are given as input parameters for the method. The main part of the method is the block dealing with ABM dynamics. Outputs from this block are current height (y) of the ABM and net power (P_{net}) and net energy (E_{net}). Information about the height is necessary for obtaining the wind speed and air density which then enters the ABM dynamics block as input parameters.

Cylinder rotation (ω) is dependent on the optimal point of lift-to-drag coefficient ratio (CF_L/CF_D) and some maximum allowable value, determined by the structural properties of the rotating cylinder.

$$\omega = \min(\omega_{\max}, X_{opt} v_{rel}/R) \tag{10}$$

$$\omega_{\max} = 2\pi n_{\max} \tag{11}$$

$$X_{opt} = f(CF_L/CF_D)_{\max} \tag{12}$$

This approach assures that we have the optimal lift-to-drag coefficient in the process. From the optimal value of X the resulting lift (F_L) and drag (F_D) force can be found, as well as moment due to friction between cylinder and air (M_{fr}), i.e. external moment required for the cylinder rotation.

Schematic view of the forces and moments acting on the ABM are given in Fig. 4. These are: ABM and cable weight ($F_{g,ABM}$ and $F_{g,c}$), ABM buoyant lift force $F_{L,Ar}$, lift F_L and drag F_D force due to

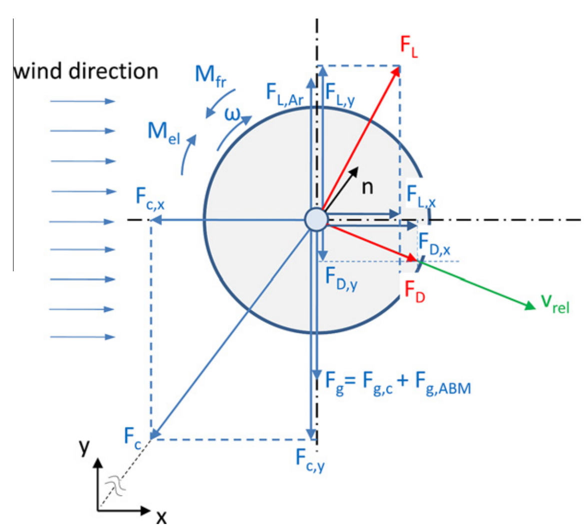

Fig. 4. Forces and moments acting on the ABM. Note that direction of F_D is not aligned with the main axis (x), but with the axis pointing in the direction of v_{rel}. F_L is, as always, perpendicular to F_D.

rotation of the cylinder in wind, cable pulling force F_c. Sum of these forces gives the resulting force F_r acting on ABM, see Eq. (13). Cable puling force is the reactive force of the winch system. During the power production phase it should have the opposite orientation than velocity of the ABM, i.e. it tends to suppress ABM movement. During the recovery phase those forces should point in same direction, i.e. cable force is pulling the ABM back to origin. During the power production phase, cable force should be sufficiently high because it is directly proportional to power production (resistance against the upward movement). During the recovery phase it should be as low as possible in order to reduce energy consumption (pull-down force), but strong enough to ensure return of the ABM into the starting position. In reality, cable force should be constrained to the value of the cable tensile strength, but this constrain is not taken into account here.

The direction of the lift and drag force are always dependent on a relative velocity between ABM movement and apparent wind velocity, see Fig. 5.

During the production phase resulting force points away from the ground winch system and ABM is moving away from the winch system. During the recovery phase, resulting force points towards the winch system. Also, during this phase cable force should be minimized. This force is also responsible for ABM acceleration and its velocity and position change in time:

$$\vec{a} = \frac{1}{m}\sum \vec{F} = \frac{1}{m}(\vec{F}_w + \vec{F}_c + \vec{F}_g + \vec{F}_l) \tag{13}$$

$$\vec{v} = \int_\tau \vec{a}dt \tag{14}$$

$$\vec{x} = \int_\tau \vec{v}dt \tag{15}$$

Moments acting on ABM are: moment M_{el} provided by electro motor (EM) driving the ABM and aerodynamic friction moment M_{fr} from cylinder rotation (Fig. 6). For the simplicity, in this work it is assumed that they are in balance during the process.

During the production phase new cable length can be updated after each time step:

$$\vec{L}_c = \int_\tau \vec{v}dt \tag{16}$$

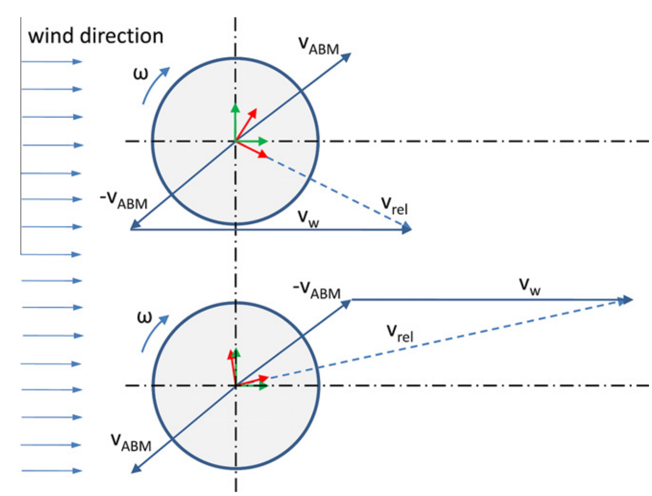

Fig. 5. Relationship between ABM velocity, wind velocity and relative velocity for the production (upper figure) and recovery (lower figure) phase. The green represents reference x–y coordinate system, while red represents drag-lift coordinate system. (For interpretation of the references to color in this figure legend, the reader is referred to the web version of this article.)

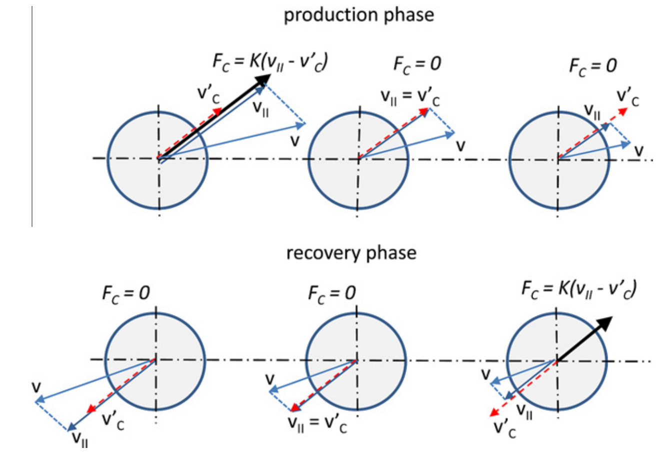

Fig. 6. Winch cable pulling force dynamics for both production and recovery phase.

It is reasonable to limit the cable length to some value. Therefore, production cycle ends if:

- ABM goes above some allowable height, or
- Cable unwinds to the end.

Weight forces acting on ABM are the weight of the cable ($F_{g,c}$) and ABM ($F_{g,ABM}$) itself. ABM weight is roughly estimated as weight of the cast (cast surface times specific weight of the cast material) with added weight of the EM. Balance of weight forces in given in Eq. (17). Due to the fact that cable is not transmitting pressure forces, the assumption is that complete weight of the cable is acting on the ABM, pulling it down, Eq. (18).

$$F_{g,ABM} = (2R\pi + 2R^2\pi)q_{g,cast} + 2F_{g,EM} \tag{17}$$

$$F_{g,c} = |\vec{L}_c|q_{g,c} \tag{18}$$

Buoyant force due to difference between helium and surrounding air density is calculated from the Archimedes' principle:

$$F_{L,Ar} = (\rho_{air} - \rho_{He})Vg \tag{19}$$

Force transmitted by the cable is calculated by using the equation

$$\vec{F}_c = K(\vec{v}_{II} - \vec{v}'_c) \tag{20}$$

Vector components of previous expression are related to the unit vector aligned with the axis connecting ABM and GS and pointing outwards from the GS (see Fig. 4). This vector is calculated from the current position of the ABM and under the assumption that GS is in the center of coordinate system the expression is given by

$$\vec{n} = \vec{x}/|\vec{x} + \vec{y}| + \vec{y}/|\vec{x} + \vec{y}| \tag{21}$$

K is a model constant representing response of the electro motor (generator) inside the winch to winding/unwinding velocity from the winch drum. Velocities are given by following equations:

$$\vec{v}_{II} = (\vec{v}\cdot\vec{n})\vec{n} \tag{22}$$

$$\vec{v}'_c = |\vec{v}'_c|\vec{n} \tag{23a}$$

$$\vec{v}'_c = |\vec{v}'_c|(-1\cdot\vec{n}) \tag{23b}$$

Eq. (22) represents projection of the ABM velocity to normal vector. Eq. (23) represents target velocity of the cable movement, which has the pre-defined magnitude and direction pointing outwards or towards the ground station, Eqs. (23a) and (23b), depending if production or recovery phase is occurring. Magnitude of target velocity should be set to the values suitable for the unwinding/winding mechanism of the winch system.

Illustration of the principle is given in the following figure:

From the known values of the cable force and it's target velocity the power transmitted by the cable can be calculated. It has different form for production and recovery phase, Eqs. (24a) and (24b).

$$P_c = \max[0, (\vec{F}_c \cdot \vec{v}'_c)] \tag{24a}$$

$$P_c = \min[0, (\vec{F}_c \cdot \vec{v}'_c)] \tag{24b}$$

Power balance consists from power transmitted by the winch cable and losses in the electro motors of the ABM:

$$P_{net} = P_c - P_{EM} = P_c + M_{fr}\omega \tag{25}$$

Energy balance is calculated by integrating power balance over time.

$$E_{net} = \int_\tau P_{net} dt \tag{26}$$

Special attention has to be given to the recovery phase of the cycle. During the recovery phase lift force should be set to minimum in order not to contribute to the forces resisting the downward motion. However, lift should be obtained again somewhere in the recovery phase, since ABM is not allowed to fall down to the ground, but has to return to origin. This can be done with incorporating a simple regulation loop in the system. For instance, in this work the falling of the ABM to the ground is prevented by employing the rotation of the cylinder when angle α between the ABM, origin of the system and line following the ground falls below some critical value. Logistic function, as a smooth approximation of Heaviside function, is used:

$$\omega = 1 - 1/(1 + \exp(-2C(\alpha - \alpha'))) \tag{27}$$

In Eq. (27) C represents model constant.

3. Results and discussion

3.1. Overview of simulation parameters and simulation set-up

CFD analysis is based on 2D calculations, with cylinder radius of 3.5 m. The three supercritical Re numbers used in this work are 10^6, 5×10^6 and 10^7. The spin ratio values are going from zero (non-rotating cylinder) to spin ratio corresponding to cylinder's maximum allowable rotating frequency. The matrix that summarizes set-up for CFD calculations is given in Table 1. The calculation mesh can be seen in Fig. 7.

Table 1
Matrix showing calculation points (noted by letter 'c') where CFD analysis of aerodynamic coefficients was performed. Interpolated points are noted by letter 'i'.

$X\downarrow$ Re$\rightarrow$	10^6	$5\cdot10^6$	10^7
0	c	c	c
0.05	i	i	i
0.1	i	c	c
0.2	i	c	i
0.25	i	i	c
0.4	i	i	i
0.5	c	c	c
0.7	i	i	c
1	c	c	
1.4	i	c	
2.5	c		
5	c		
7	c		

Since wind speed magnitude is probably the most important technical parameter of the process, results will be provided for three different cases with increasing velocity magnitude w.r.t. the reference wind profile, as presented in Table 2. The reference wind profile is given in Fig. 8. Input parameters for the process dynamics modelling are:

- Wind speed profile is following wind power density given by Archer and Caldera in 2009 [6] and it follows wind speed profile which occurs in 5% of the time, averaged over the entire world (Fig. 8) with three different cases (see Table 2).
- Cylinder dimensions: 3 m in radius and 30 m in length.
- Cylinder top position should not exceed 2000 m in height, nor fall below 50 m.
- Maximum cylinder rotating frequency is set to 2 s^{-1}.
- Maximum cable length is 2500 m.
- Model constant for cable pulling force (K) is estimated to 10^6 N s/m.
- Specific weight of the cable was set to 50 N/m; weight of the cast was estimated to 10 N/m^2; the weight of the electro motors was set to 2×200 N.
- Magnitude of threshold velocity is estimated to the value of 4 m/s for power production and 6 m/s for the recovery phase. The difference in values comes from the fact that during the recovery phase lower cable force is expected. Increased threshold velocity in recovery phase also shortens time needed to complete the whole cycle.
- Model constant for logistic function of the regulation in the recovery phase is set to 10.
- Critical angle in the recovery phase regulation, see Eq. (27), is set to 10 deg.

All results are presented on the basis of one cycle, i.e. one production phase followed by one recovery phase. This is possible since proposed concept of power production is anyway discontinuous process. Analysis based on one cycle is sufficient to give information about feasibility of the process, as well to provide differences between cases. Main result is the net power production per-cycle. Furthermore, information about resulting power and all forces modelled in the process is given. In addition to that cylinder rotation and trajectories of the ABM movement is given.

3.2. Discussion of results

3.2.1. CFD analysis

The illustrative representation of the converting drag to lift via cylinder rotation is given by Fig. 9.

In Fig. 9a the field of the pressure around non-rotating cylinder is oscillating around zero value thus providing no overall average

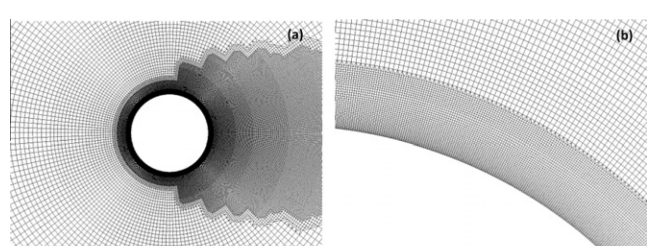

Fig. 7. Calculation mesh for CFD simulation. (a) Mesh around the cylinder; (b) mesh in the boundary layer region.

Table 2
Difference between three cases under investigation.

Name	Description
Case 1	Reference case – wind profile given in Fig. 8
Case 2	20% Higher wind speed than in reference case
Case 3	40% Higher wind speed than in reference case

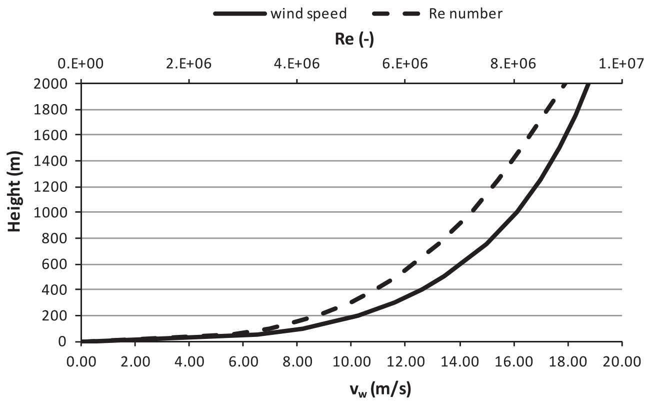

Fig. 8. Wind magnitude and density as a function of height.

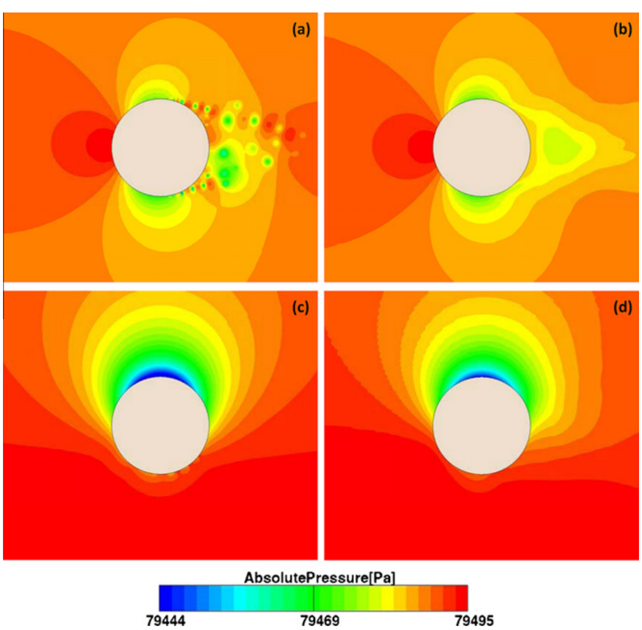

Fig. 9. Results of two-dimensional CFD studies for Re = 1e6. Free-stream wind direction is from left to right. (a) Instantaneous pressure field for non-rotating cylinder, $X = 0$; (b) time averaged pressure field for non-rotating cylinder, $X = 0$; (c) instantaneous pressure field for rotating cylinder, $X = 5$; (d) time averaged pressure field for rotating cylinder, $X = 5$.

lift force. Vortex shedding can be seen as vortices are present in low-pressure areas (also known as von Karman vortices). The vortex shedding frequency process suppresses with increase in cylinder rotation [39,40] and finally diminishes at sufficiently high values of X. When cylinder rotates, see Fig. 9b, it damps the oscillations of the lift force and stabilizes the high pressure field slightly below the cylinder thus enabling positive lift force of the process. Development of drag and lift coefficients in time can be seen in Fig. 10.

Validation of the CFD procedure, which is described in Section 2.1.1, was done by comparing calculated drag coefficients for

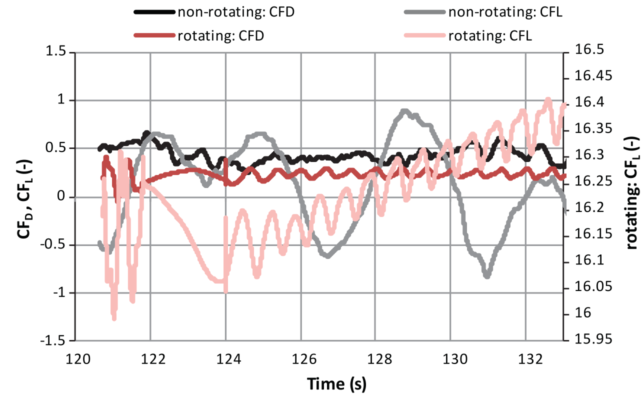

Fig. 10. Simulation results of drag and lift coefficients in time for Re = 1e6. Spin ratio for non-rotating cylinder is $X = 0$ and for rotating cylinder, $X = 5$.

non-rotating cylinder in supercritical region (where Re number is above 10^6). Results are presented in Fig. 11. By authors' knowledge, results of drag coefficients presented in this work (Fig. 11) are, up to date, the first numerically calculated drag coefficients which are following the trend obtained by experiments in supercritical region up to Re = 10^7.

Figs. 12–15 summarizes results of required coefficients computed by CFD analysis.

Results presented in Figs. 12–14 are incorporated into the look-up tables which are then used in the simulation of the process.

From Fig. 15 it can be seen that lift-to drag coefficient ratio is rising with the increasing spin ratio X, and has highest value around $X = 7$, which makes it the optimal spin ratio (X_{opt}). Under the condition of optimal spin ratio the production phase will be the most efficient, i.e. cylinder rotation-to-relative velocity ABM will tend to go highest possible with the lowest demanding energy. However, keeping the spin ratio in optimal value could result in rotating frequency of the cylinder above the maximal allowable value.

3.2.2. Process dynamics

Power on the winch system is highest in Case 3 (Fig. 16). It can be seen that winch power amount is positively correlated with the available wind speed. Peak power in the Case 3 is above 1 MW, and in Case 1 above 400 kW. The net power production is highest in the Case 3 (Fig. 17). Results for net power and energy are expected, since wind speed magnitude is the only potential for generating cable force during the power production cycle. For Case 1 there is a flat line at the value of zero in power production cycle. This is due to the process criteria to stop the production cycle w.r.t.

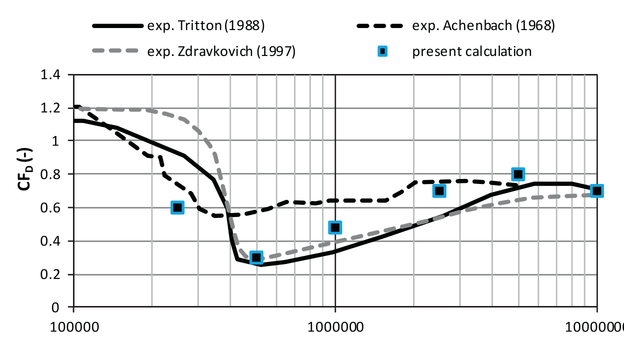

Fig. 11. Simulation results of drag coefficients vs. Re number for non-rotating cylinder. Results are compared with experimental results of Achenbach [41], Tritton [42] and Zdravkovich [43].

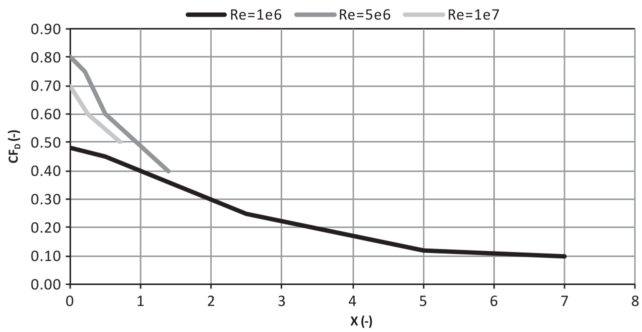

Fig. 12. Drag coefficient vs. spin ratio with Re number as parameter.

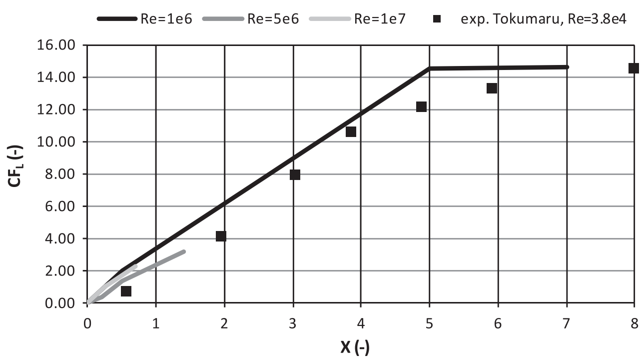

Fig. 13. Lift coefficient vs. spin ratio with Re number as parameter. Results are compared with experiments from Tokumaru and Dimotakis [44].

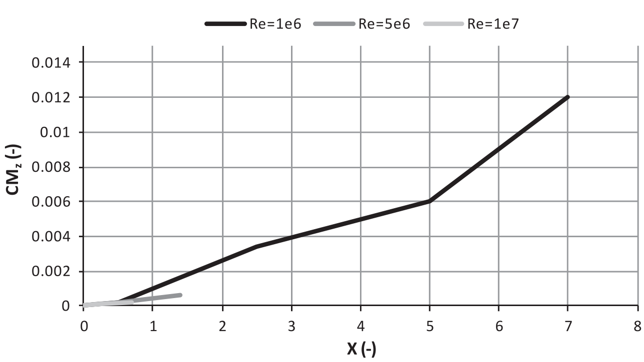

Fig. 14. Moment coefficient vs. spin ratio with Re number as parameter.

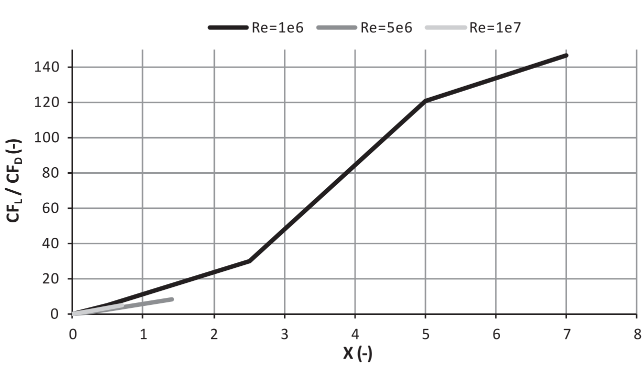

Fig. 15. Lift-to-drag coefficient vs. spin ratio with Re number as parameter.

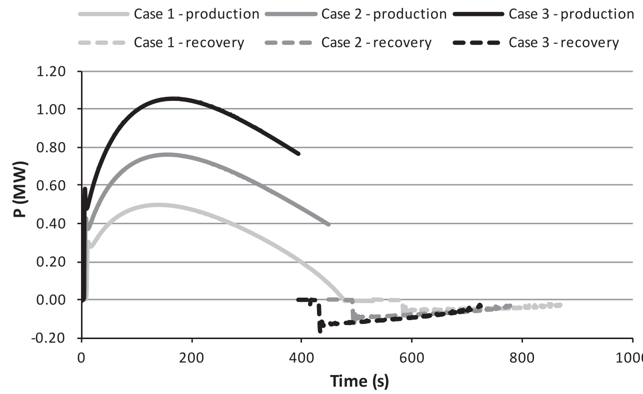

Fig. 16. Net power during the complete cycle (production and recovery phase) for all three cases.

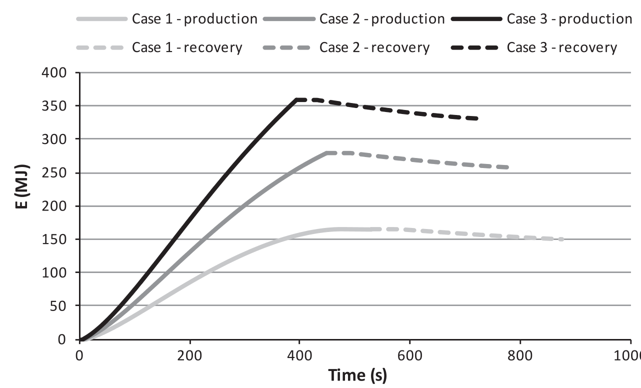

Fig. 17. Net energy during the complete cycle (production and recovery phase) for all three cases.

maximum values of ABM height or cable length, which should be improved by some other criteria, like actual end of power production. Crucial information for all cases is the production-to-recovery energy balance, i.e. how much of the gained energy from the production phase must be spent during the recovery phase for pulling the ABM to starting position. The aim is to have this value as low as possible. In all cases it is below 8%, which is meaning that 92% of energy obtained in production phase can be used on the winch. Duration of the process is also important outcome of the simulations. It can be seen from the figures that the difference between longest (Case 1) and shortest (Case 3) cycle is approx. 140 s. If we take into account that in Case 1 power production actually ends approx. 80 s before the production phase is over, this

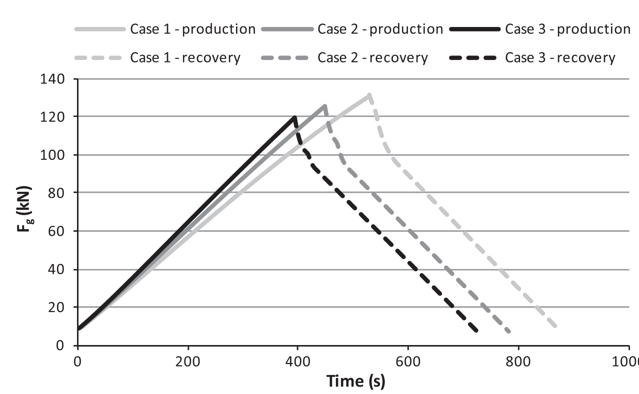

Fig. 18. Sum of weight forces acting on the ABM during the complete cycle (production and recovery phase) for all three cases.

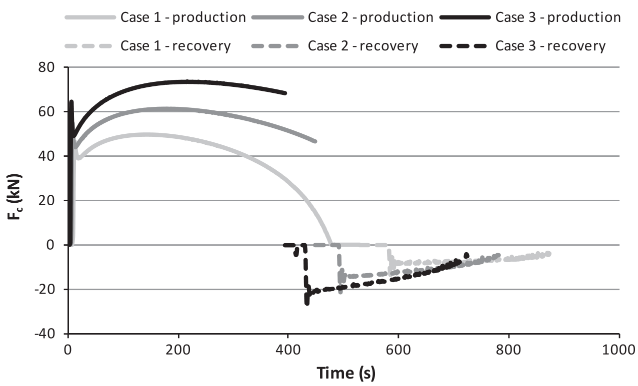

Fig. 19. Force in the cable in *x* direction during the complete cycle (production and recovery phase) for all three cases.

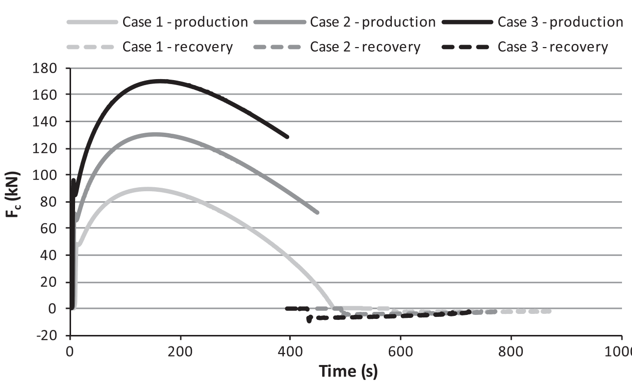

Fig. 20. Force in the cable *y* direction during the complete cycle (production and recovery phase) for all three cases.

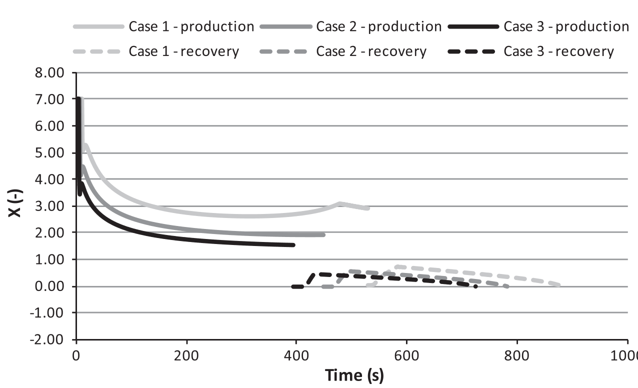

Fig. 21. Cylinder spin ratio during the complete cycle (production and recovery phase) for all three cases.

difference could in systems with enhanced regulation and control be around approx. 60 s.

Solution of the weight force is trivial (Fig. 18), since it changes only due to increase/decrease of the cable length during the production/recovery phase.

Magnitude of the cable force in *x* and *y* direction (Figs. 19 and 20) are following the trend of power curve, Fig. 16. The signs of cable force components are represented in Fig. 7. Positive value in production phase is the value which is available for power production on the winch when ABM is moving away from with production phase v_c'. Negative value in recovery phase represents force which has to be provided by the winch system in order to pull

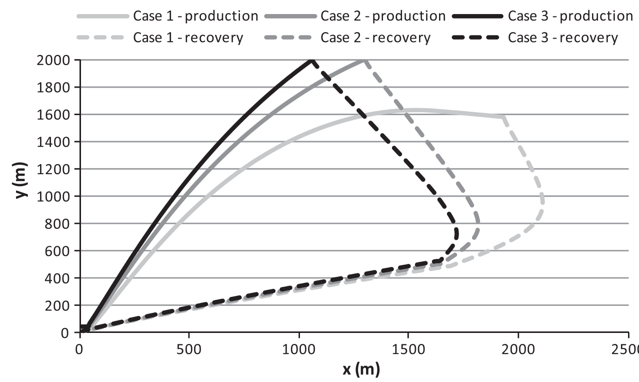

Fig. 22. Trajectories of ABM movement during the complete cycle (production and recovery phase) for all three cases.

ABM back to original position with recovery phase v_c'. It can also be seen that during the production phase the *y* component of the cable force is more than twice larger than the *x* component. During the recovery phase the *x* component of cable force is roughly twice larger than the *y* component.

Cylinder rotation determines how much of the wind force will be converted from *x*-direction to *y*-direction. Fig. 21 represents the spin ratio during the complete cycles for all cases. For all cases, during the production phase spin ratio is always below an optimal value of $X_{opt} = 7$. This is due to limitation in cylinder rotation rate. Spin ratio in recovery phase is small since it only has to provide lift for keeping the ABM airborne, without the need for obtaining positive cable force.

Trajectories for all cases, Fig. 22, are showing that significant differences in production and recovery phase. In Case 1 the ABM did not reach the predefined top value of 2000 m. It's production cycle ended when cable force decreased to zero. ABM reaches minimum horizontal distance from GS in Case 3, and maximum in Case 1. Ratios between reached height vs. horizontal distance are 0.82, 1.54 and 1.88 for Case 1, Case 2 and Case 3. It is also interesting to see that trajectories for all three cases eventually collide during the recovery phase.

4. Conclusion

This paper attempts to describe feasibility of the Magnus' effect-based concept for utilizing high altitude wind power potential. The presented model is divided into CFD and process dynamics part. Each of the two parts carries it's own simplifications and assumptions. Due to that fact, results presented in this study should be taken with certain reserve whose magnitude will not be known until actual field measurements on real prototype will be available. However, complete modelling presented in this work is based on successfully validated CFD methodology and well-known physical laws of motion, thus making this study reasonably valid for concluding on concept's feasibility.

- LES-CSM framework of CFD calculations is successful in obtaining accurate drag coefficient for supercritical values of Re number in the case of non-rotating cylinder ($X = 0$).
- For $X > 0$, calculated dependence of lift coefficient on spin ratio is similar for complete span of Re numbers, taking into account that spin ratio is limited to the maximum rounds-per-minute of the cylinder.
- For $X > 0$, calculated dependence of lift coefficient on spin ratio for high Re numbers shows the same trend as experiment performed on low Re-number.

Process dynamics is showing that power production and energy balance between production and recovery phase in Magnus' concept depends strongly on wind speed magnitude:

- In all three cases the net energy, given by the sum of energies from the production and recovery phase, is positive thus indicating that power production from high altitude winds with the presented concept is possible.
- Increase in wind speed increases net energy and process efficiency, i.e. ratio between energy gained in production vs. energy spent in the recovery phase.
- Increase in wind speed shortens time of the production phase and time of the overall cycle.
- On the other hand, increase in wind speed increases force which should be transmitted by the cable.
- With the given wind speed and limitation in cylinder rotation, spin ratio rapidly decreases just after the start of the production phase.

The most important improvements, which should be under consideration for future studies are: more realistic regulation of the process, introduction of third dimension into considerations, and introduction of the additional model constraints, mainly related to winch cable tensile strength limit (which will demand even more complicated regulation).

Acknowledgements

This work has been done with the support of Omnidea Lda, Portugal, who originally developed the concept. The concept is now under the research within the project High Altitude Wind Energy (acronym HAWE), with the financial support of EC's Seventh Framework Programme (RCN 96067). Also, authors would like to thank the Automotive Mechatronics Group of Faculty of Mechanical Engineering and Naval Architecture (University of Zagreb) for providing useful discussion about the Magnus' concept. NCEP_Reanalysis 2 data provided by the NOAA/OAR/ESRL PSD, Boulder, Colorado, USA, from their Web site at www.esrl.noaa.gov/psd/ (last access 5th of April 2012).

References

[1] Chang TH, Huang CM, Lee MC. Threshold effect of the economic growth rate on the renewable energy development from a change in energy price: evidence from OECD countries. Energy Policy 2009;37:5796–802.
[2] Marques AC, Fuinhas JA, Manso JRP. Motivations driving renewable energy in European countries: a panel data approach. Energy Policy 2010;38:6877–85.
[3] Menz FC, Vachon S. The effectiveness of different policy regimes for promoting wind power: experiences from the states. Energy Policy 2006;34:1786–96.
[4] Bronstein MG. Harnessing rivers of wind: a technology and policy assessment of high altitude wind power in the US. Technol Forecast Soc 2011;78:736–46.
[5] Arya S. Introduction to micrometeorology. New York: Academic press; 1988.
[6] Archer CL, Caldeira K. Global assessment of high-altitude wind power. Energies 2009;2:307–19.
[7] Kanamitsu M, Ebisuzaki W, Woollen J, Yang SK, Hnilo JJ, Fiorino M, et al. Ncep-doe amip-ii reanalysis (R-2). Bull Am Meteorol Soc 2002;83:1631–43.
[8] Hagspiel S, Papaemannouil A, Schmidt M, Andersson G. Copula-based modeling of stochastic wind power in Europe and implications for the Swiss power grid. Appl Energy 2011. http://dx.doi.org/10.1016/j.apenergy.2011.10.039.
[9] Magenn Power Inc. <www.magenn.com/technology.php> [accessed 12.04.12].
[10] Lansdorp B, Ockels WJ. Comparison of concepts for high-altitude wind energy generation with ground based generator. In: 2nd China international renewable energy equipment & technology exhibition and conference. Beijing; 2005.
[11] Roberts BW, Shepard DH, Caldeira K, Cannon ME, Eccles DG, Grenier AJ, et al. Harnessing high-altitude wind power. IEEE Trans Energy Convers 2007;22:136–44.
[12] Loyd ML. Crosswind kite power. J Energy 1980;4:106–11.
[13] Argatov I, Rautakorpi P, Silvennoinen R. Estimation of the mechanical energy output of the kite wind generator. Renew Energy 2009;34:1525–32.
[14] Argatov I, Silvennoinen R. Energy conversion efficiency of the pumping kite wind generator. Renew Energy 2010;35:1052–60.
[15] Fagiano L. Control of tethered airfoils for high-altitude wind energy generation. PhD thesis. Politechnico di Torino; 2009.
[16] Canale M, Fagiano L, Milanese M. KiteGen: a revolution in wind energy generation. Energy 2009;34:7.
[17] Argatov I, Rautakorpi P, Silvennoinen R. Apparent wind load effects on the tether of a kite power generator. J Wind Eng Ind Aerod 2011;99:1079–88.
[18] Krajačić G, Duić N, Tsikalakis A, Zoulias M, Caralis G, Panteri E, et al. Feed-in tariffs for promotion of energy storage technologies. Energy Policy 2011;39:1410–25.
[19] Ćosić B, Markovska N, Krajačić G, Taseska V, Duić N. Environmental and economic aspects of higher RES penetration into Macedonian power system. Appl Therm Eng 2011. http://dx.doi.org/10.1016/j.applthermaleng.2011.10.042.
[20] Chen FZ, Duić N, Alves LM, da Graca Carvalho M. Renewislands – renewable energy solutions for islands. Renew Sustain Energy Rev 2007;11:1888–902.
[21] Duić N, Krajačić G, Carvalho MD. RenewIslands methodology for sustainable energy and resource planning for islands. Renew Sustain Energy Rev 2008;12:1032–62.
[22] Lund H, Duić N, Krajačić G, Carvalho MD. Two energy system analysis models: a comparison of methodologies and results. Energy 2007;32:948–54.
[23] Busuttil A, Krajačić G, Duić N. Energy scenarios for Malta. Int J Hydrogen Energy 2008;33:4235–46.
[24] Krajačić G, Duić N, Carvalho MD. How to achieve a 100% RES electricity supply for Portugal? Appl Energy 2011;88:508–17.
[25] Segurado R, Krajačić G, Duić N, Alves L. Increasing the penetration of renewable energy resources in S. Vicente, Cape Verde. Appl Energy 2011;88:466–72.
[26] Mathiesen BV, Lund H, Karlsson K. 100% Renewable energy systems, climate mitigation and economic growth. Appl Energy 2011;88:488–501.
[27] European Commission Community Research and Development Information Service (CORDIS). <http://cordis.europa.eu/fetch?CALLER=FP7_PROJ_EN&ACTION=D&DOC=1&CAT=PROJ&RCN=96067> [accessed 15.10.11].
[28] Magnus G. On the deviation of projectiles, and: on a sinking phenomenon among rotating bodies. Ann Phys 1853;164:29.
[29] Aoki K, Ito T. Flow characteristics around a rotating cylinder. Proc School Eng Tokai Univ 2001;26:6.
[30] Karabelas SJ, Koumroglou BC, Argyropoulos CD, Markatos NC. High Reynolds number turbulent flow past a rotating cylinder. Appl Math Model 2012;36:379–98.
[31] Karabelas SJ. Large Eddy simulation of high-Reynolds number flow past a rotating cylinder. Int J Heat Fluid Flow 2010;31:518–27.
[32] Breuer M. A challenging test case for large eddy simulation: high Reynolds number circular cylinder flow. Int J Heat Fluid Flow 2000;21:648–54.
[33] Catalano P, Wang M, Iaccarino G, Moin P. Numerical simulation of the flow around a circular cylinder at high Reynolds numbers. Int J Heat Fluid Flow 2003;24:463–9.
[34] Breuer M. Numerical and modelling influences on large eddy simulations for the flow past a circular cylinder. Int J Heat Fluid Flow 1998;19:10.
[35] Singh SP, Mittal S. Flow past a cylinder: shear layer instability and drag crisis. Int J Numer Methods Fluids 2005;47:75–98.
[36] Mittal S. Computation of three-dimensional flows past circular cylinder of low aspect ratio. Phys Fluid 2001;13:177–91.
[37] Braza M, Chassaing P, Minh HH. Prediction of large-scale transition features in the wake of a circular-cylinder. Phys Fluids A Fluid 1990;2:1461–71.
[38] Kobayashi H. The subgrid-scale models based on coherent structures for rotating homogeneous turbulence and turbulent channel flow. Phys Fluid 2005:17.
[39] Lam KM. Vortex shedding flow behind a slowly rotating circular cylinder. J Fluids Struct 2009;15:18.
[40] Dol SS, Kopp GA, Martinuzzi RJ. The suppression of periodic vortex shedding from a rotating circular cylinder. J Wind Eng Ind Aerod 2008;96:1164–84.
[41] Achenbach E. Distribution of local pressure and skin friction around a circular cylinder in cross-flow up to $Re = 5 \times 10^6$. J Fluid Mech 1968;34:625–39.
[42] Tritton DJ. Physical fluid dynamics. 2nd ed. New York: Oxford University Press USA; 1988.
[43] Zdravkovich MM. Flow around circular cylinders: fundamentals, vol. 1. New York: Oxford University Press USA; 1997.
[44] Tokumaru PT, Dimotakis PE. The lift of a cylinder executing rotary motions in a uniform-flow. J Fluid Mech 1993;255:1–10.